

## Calculated Electron Dynamics in a Strong Electric Field

F. Robicheaux and J. Shaw

*Department of Physics, Auburn University, Auburn, Alabama 36849*

(Received 6 August 1996)

The *dynamics* of an electron wave attached to  $\text{Rb}^+$  is calculated when the atom is in a strong electric field. The dynamic motion of the electron is generated by exciting Rb from its ground state using a weak, pulsed laser. We compare the quantum results for  $m = 0$  to recent experiments. The comparison requires a calculation of the electron flux at a macroscopic distance from the atom. We discuss some of the interesting aspects of this problem including trimming autoionizing states, interference patterns downfield, and suppression of downfield scattering. [S0031-9007(96)01637-7]

PACS numbers: 34.80.Kw, 31.10.+z, 31.30.Jv

Atomic physics is a mature field and the study of electronic processes has been of central concern since the beginning. This study of electronic processes has mainly proceeded through the exploration of phenomena at a fixed energy; i.e., in the frequency domain. Recent technological advances have allowed the creation and detection of electron wave packets [1–11] in atoms. In these experiments, the electronic wave function has nontrivial time dependence giving atomic processes in the time domain. However, in order to make wave packets at all, most of these studies were for simple systems.

Nevertheless the study of electron wave packets is fascinating because it is relatively simple to connect this exact quantum description of the world to our approximate, but finely honed, classical intuition. Often, features in exact quantum wave packets can be related to specific classical processes. This is not too surprising since quantum dynamics generates the classical mechanics. Still it is wonderful to see, in one system, behavior that can be interpreted classically and behavior that must be interpreted quantum mechanically.

In this paper we present the results of our calculations that describe the complex dynamics of electron waves in strong, static electric fields. The electron wave packet is generated by shining weak, pulsed light on Rb in a static electric field. This system may be considered a prototype for the extension of wave packet studies to more than one dimension: The motion of the electron is nearly separable in two coordinates with the motion in each direction strongly coupled over a limited spatial region. We have compared our calculations to the experimental results obtained by Lankhuijzen and Noordam [11]; there was excellent agreement for all comparisons. This experiment provides a new challenge to theory in that they excite autoionizing states and measure the time dependence of the electron flux that is naturally ejected from the atom. This means calculations must be quite sophisticated in order to account for the nonperturbative effect of the electric field on the electron's dynamics and to account for the electron moving a macroscopic distance from the nucleus to the detector.

The static electric field gives a potential  $F_{\text{stat}} \cdot z$  in addition to the potential the electron experiences from the nucleus and the core electrons. On the  $z$  axis the electron's potential increases monotonically to infinity as  $z$  increases from the origin; no electron can escape upfield. In the downfield direction, the electron's potential increases until  $z = -1/\sqrt{F_{\text{stat}}}$  then decreases to minus infinity as  $z$  decreases from the origin. This humped shape forms a barrier to electron escape to minus infinity. In an electric field, all atomic states become resonances because the electron can tunnel through the barrier to  $z = -\infty$ . However, these tunneling times are extremely long for energies less than  $E_c = -2\sqrt{F_{\text{stat}}}$ .  $E_c$  is the lowest energy at which a classical electron can go over the barrier. For energies larger than  $E_c$ , a classical electron can go over the top of the barrier provided it does not have too much energy tied up in "transverse" motion.

The quantum and classical dynamics is most easily described in parabolic coordinates because the Hamiltonian for an H atom in a static electric field separates in these coordinates. The motion is bounded in the  $\xi = r + z$  coordinate and unbounded in the  $\eta = r - z$  coordinate. Since the electron escapes in the  $\eta$  direction we will consider motion in the  $\xi$  direction to be transverse to the escape motion. The azimuthal quantum number  $m$  and the number of nodes in the wave function in the  $\eta$  direction define a channel for this system. The electron must tunnel through a barrier to leave the atom in every channel for energies less than  $E_c$ . For energies greater than  $E_c$ , the electron can escape directly over the barrier in the channels with few nodes in the wave function in the  $\xi$  direction but the electron must tunnel through the barrier to escape in the channels with many nodes in the  $\xi$  direction. As the energy increases above  $E_c$  more channels become open. For long-lived resonances in closed channels, we can count the number of nodes in the wave function in the  $\xi$  direction,  $n_\xi$ , and the number of nodes in the wave function in the  $\eta$  direction,  $n_\eta$ , to classify the resonance state; the principal quantum number is  $n = n_\xi + n_\eta + |m| + 1$ .

In all cases of excitation by a weak laser (no multi-photon transitions), the wave packet is the solution of the

inhomogeneous wave equation (in atomic units)

$$\left(i \frac{\partial}{\partial t} - H\right)\psi(\vec{r}, t) = \hat{\epsilon} \cdot \vec{r}F(t) \cos \omega t \psi_I(\vec{r}, t), \quad (1)$$

where  $H$  is a time independent Hamiltonian,  $\omega$  is the main laser frequency, and  $F(t)$  is the amplitude of the electric field at the nucleus generated by the laser field. For the process described in this paper,  $H$  is the Rb atomic Hamiltonian plus a term from the static electric field. There are many formally equivalent ways of obtaining the  $\psi$  function describing the wave packet. The two methods used in this work involve the linear superposition of the continuum of solutions of the homogeneous Schrödinger's equation at a fixed energy and the linear superposition of the solutions of the inhomogeneous Schrödinger's equation at a fixed energy. We use both methods because it is easier to obtain the asymptotic flux by superposing the homogeneous functions (allowing comparison with experiment), but it is easier to obtain the wave function near the nucleus ( $r < 2000$  a.u.) by superposing the inhomogeneous functions (allowing visualization of the dynamics).

The homogeneous wave functions and the dipole matrix elements are obtained in parabolic coordinates using a method based on that developed by Harmin [12] and Fano [13]. The wave function near the core is given in terms of the field free wave functions since the static electric field is small ( $F_{\text{stat}} \sim 4 \times 10^{-7}$  a.u.  $\sim 2$  kV/cm). These functions are accurately known because the quantum defects  $\mu_\ell$  are accurately known from the bound states of Rb. In Rb, the quantum defects for  $\ell \geq 3$  are effectively 0; thus Rb differs from hydrogen for  $\ell \leq 2$ . By matching the solutions in spherical coordinates near the core to the solutions in parabolic coordinates outside of the core region, the wave function at all points in space may be obtained. The  $\text{Rb}^+$  core electrons break the parabolic symmetry for the valence electron and can scatter it from one parabolic channel to another. In the energy range that is being examined, this is the main mode of decay. For Rb, the electron has a much higher probability of escaping by scattering into channels with low transverse energy than by tunneling through the barrier.

In a recent experiment [11], the time dependent flux of electrons was measured from a Rb atom in  $\sim 2$  kV/cm constant electric field. In this experiment, the electron wave packet was created by excitation of Rb out of its ground state into states above the classical ionization threshold using a weak pulsed laser. The pulse duration has a FWHM of  $\sim 4.8$  ps. We were able to obtain good agreement with their experimental results for all of the cases they examined. We present detailed comparison for only one of their geometries.

In Fig. 1, we present the energy dependent cross section and the amplitude for finding a photon at each energy as a function of the energy below the zero field threshold. The form of  $\mathcal{F}(E)$  (the amplitude for finding a photon at an energy to raise the atom to energy  $E$ ) was chosen to be  $\exp\{-(E - E_0)/\Gamma\}^4$ . For this cal-

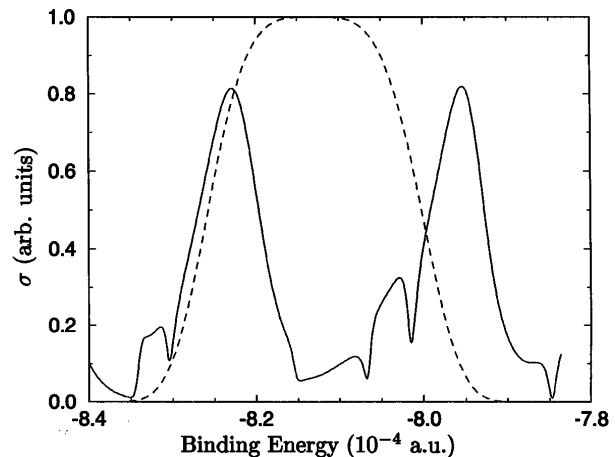


FIG. 1. Solid line: Proportional to the infinite resolution photoionization cross section as a function of the electron's energy:  $F_{\text{stat}} = 1985$  V/cm and  $m = 0$ . Dashed line: Proportional to  $\mathcal{F}(E)$ , the amplitude for finding a photon at each energy.

ulation the laser is polarized parallel to the static field,  $F_{\text{stat}} = 3.86 \times 10^{-7}$  a.u. = 1985 V/cm,  $E_0 = -8.13 \times 10^{-4}$  a.u., and  $\Gamma = 1.4 \times 10^{-5}$  a.u. (corresponding to a 2.4 ps half-width pulse duration). The two main structures in the relevant energy range are the  $n_\xi = 20, n_\eta = 1$  ( $n = 22$ ) state at  $-7.95 \times 10^{-4}$  a.u. and the  $n_\xi = 19, n_\eta = 2$  ( $n = 22$ ) state at  $-8.23 \times 10^{-4}$  a.u. ( $n_\xi \gg n_\eta$  indicates these states are strongly localized upfield.) In hydrogen, states strongly localized upfield decay orders of magnitude more slowly than states with  $n_\xi \sim n/2$ . In Rb, these states decay quickly because they contain a large amount of low  $\ell$  character that can scatter off the core electrons and leave the system downfield. The other structures are from states of higher  $n$  but smaller  $n_\xi$ . In Fig. 2 we plot the time dependent flux into a detector a macroscopic distance from the atom. The solid line is the experimental results of Ref. [11] and the dashed line is the calculated flux convolved with a Gaussian in time with a 1 ps FWHM. The time origin has been shifted so  $t = 0$  corresponds to the first peak. The inset shows the classical orbit that mainly contributes to the flux ejected near 7 ps; this orbit is more fully discussed below.

The first peak arises from electrons that are initially excited downfield; these electrons travel directly to the detector. The later peaks arise from the two different "angular" states beating against each other. The first recurrence peak at 7 ps is the largest because these autoionizing states decay very quickly. Note that the expected period given by  $\tau = 2\pi/\Delta E$  gives a value of 5.4 ps, which is substantially smaller than the observed value of 7.3 ps; this difference was unexplained in Ref. [11]. The difference between the expected and observed period demonstrates a qualitative distinction between wave packets constructed from discrete states versus autoionizing states. The beat period between two discrete states cannot be changed by changing the properties of the exciting laser. In contrast, the beat period between two autoionizing states can

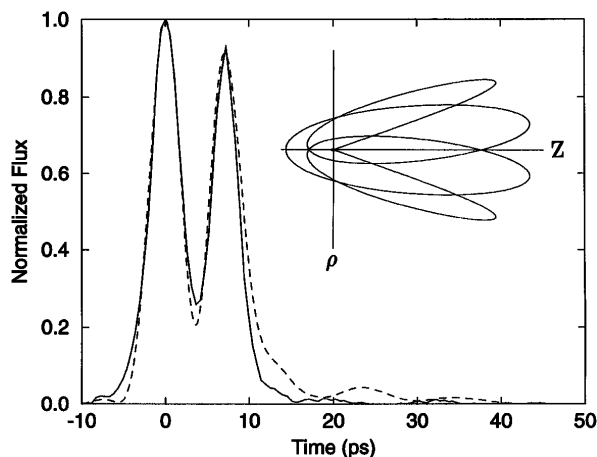


FIG. 2. The calculated (dashed line) and experimental (solid line) time dependent flux of ejected electrons (normalized to 1 at the first peak) for the parameters in Fig. 1;  $t = 0$  is set at the peak of the first pulse. The inset shows the classical orbit mainly responsible for the flux ejected near 7 ps; continuation of the orbit to negative  $\rho$  is shown to ease the visualization of this trajectory.

easily be changed if the autoionizing states are broad. This is accomplished by trimming part of the state. For example, in Fig. 1 only part of the  $n_\xi = 20, n_\eta = 1$  state at  $-7.95 \times 10^{-4}$  a.u. is excited by the laser. The trimming effectively moves this state to lower energy which decreases  $\Delta E$ . A pulse centered at  $-8.09 \times 10^{-4}$  a.u. with a width  $\Gamma = 1.7 \times 10^{-5}$  a.u. gives a recurrence time of 6.3 ps. The shape of the excitation pulse controls the beat period of two autoionizing states.

In Ref. [11], the two pulse structure of Fig. 2 was interpreted classically in that the electric field causes a precession of the electron out of  $\ell = 1$  into higher angular momentum. While the electron is in high  $\ell$ , it cannot scatter from the core and escape downfield. After an angular precession period, the electron is back in low  $\ell$  and can scatter downfield. This interpretation is exactly correct. By analyzing the calculated wave packet, we found that the probability for the electron to be within 30 a.u. of the nucleus and in  $\ell \leq 2$  was relatively large near 0 and 7 ps and relatively small at other times.

We did a detailed classical calculation to confirm and extend this interpretation. Classical trajectories were started on a spherical surface at 10–20 a.u. from the nucleus, outside the core where the potential consists of the residual Coulomb interaction and the electric field. We set the energy  $E$  to the central energy  $E = E_0$  of the laser pulse and the momentum to be perpendicular to the initial surface, so that the trajectories correspond to the rays of outgoing wave fronts that start near the origin. Given these initial conditions, the trajectories were evolved using Hamilton's equations of motion. The trajectories divide into two broad families: bound and unbound. There is a separatrix in the classical motion that starts at a critical angle  $\theta_c$  near the origin, whose location depends on the energy and electric field strength, Ref. [14]. At the energy  $-8.13 \times 10^{-4}$  a.u. and

the field strength 1985 V/cm any trajectory launched at angles greater than  $81.8^\circ$  from the  $+z$  axis will escape over the saddle and ionize, while any orbit launched at angles less than  $81.8^\circ$  will remain trapped in the vicinity of the atom until it scatters from the core. Since the separatrix is near  $90^\circ$  and the laser is polarized parallel to the electric field, roughly half the trajectories will immediately leave the atom and half will be initially bound. This may explain why roughly half of the electrons are ejected in the first pulse in Fig. 2 and half of the electrons are ejected in later pulses.

To understand the delayed ejection, we investigated the classical bound motion near the atom. The electron is trapped in the bound region unless it tunnels or scatters off the alkali core into the unbound region. The scattering can only take place if the wave is within  $\sim 5$  a.u. of the origin. For some initial angles, the electron returns to the origin quickly. For example, if it goes directly upfield,  $\theta = 0$ , it returns to the origin in 1.25 ps. This is the shortest period closed orbit. For larger launch angles, the electron is pulled down by the electric field and pulled radially inward by the Coulomb attraction so it first gains, then loses, angular momentum while precessing about the direction of the electric field. If the precession frequency is commensurate with the radial oscillation frequency, then the electron will return to the origin after  $m$  radial and  $n$  angular oscillations.

Surprisingly, *one* closed orbit is dominant for the  $E_0$ ,  $F_{\text{stat}}$ , and polarization in this experiment although there are several orbits with periods  $\sim 5.5$  ps. Reference [14] shows that a  $3/4$  resonance has created a closed orbit which goes out near  $43.3^\circ$  and returns after executing four radial oscillations to the origin at 5.7 ps. This orbit (shown in the inset of Fig. 2) has the largest recurrence strength of any of the short period orbits in the system. Also it is not an isolated orbit, but the central orbit of a large family of trajectories that return to the core with low angular momentum. Trajectories in a range from  $20^\circ$  to  $50^\circ$  are part of this family, returning within 10 bohr of the origin with  $l \leq 4$  at times from 5.2 to 6.0 ps. This family carries a substantial part of the electron wave back to the origin, where it can be scattered by the Rb core. The 5.4 ps period from the energy level spacing of Fig. 1 closely corresponds to the 5.7 ps period of this orbit [15]. The oscillation in the angular momentum of the classical trajectories also corresponds to this time scale, which confirms the reasoning in Ref. [11]. This gives a classical interpretation of the time scales for the flux ejected from the atom.

Calculating the wave packets lets you visualize the electron wave that gives rise to the asymptotic flux. For this purpose, we calculated the wave packet by superposing the inhomogeneous functions. These functions were obtained by solving the inhomogeneous equation in a basis of 49 angular momenta and  $89 - \ell$  radial functions per  $\ell$ . The radial functions were Rb radial functions that were forced to 0 at  $r = 2800$  a.u. The outgoing wave character

of the inhomogeneous functions was enforced by adding an absorbing radial potential to the Hamiltonian.

In Fig. 3, a contour plot of  $\rho|\psi(\vec{r}, t)|^2$  is given at the times  $t = 3.5$  and  $7.5$  ps as a function of  $\rho$  and  $z$ . The top of the barrier is near  $z = -1600$  a.u. The quasistanding wave character in the upfield direction (positive  $z$ ) is clearly seen as well as the few nodes in the transverse direction. The radial standing waves are obtained because the length of the laser pulse ( $\sim 4.8$  ps) is much longer than the period of a radial oscillation ( $\sim 1$  ps). The flux escaping to negative  $z$  can be clearly seen at  $7.5$  ps and very little flux escaping at  $3.5$  ps.

A striking and unexpected feature seen in Fig. 3 is the standing wave pattern at negative  $z$ . In this region of space the electron wave should be outgoing in character and therefore one might expect the wave function to be relatively flat. This striking behavior is a manifestation of "electron interference." The classical trajectories leaving the nucleus from  $\theta_c \leq \theta \leq 180^\circ$  all go towards  $z \rightarrow -\infty$ . However, trajectories ejected just below the critical angle first go out from the nucleus, reach a turning point in  $\rho$  where they fold over themselves, and are then pulled around below the nucleus back towards the negative  $z$  axis by the Coulomb attraction. Since  $\rho$  is defined positive, they cannot cross the  $z$  axis, but reflect out again while falling in the electric field. As the ejection angle increases, the trajectories touch the turning point in  $\rho$  further and further down the  $z$  axis. Since the trajectory field folds over itself, it is possible to get interference patterns in the outgoing waves because there is always more than one path reaching the same point in space.

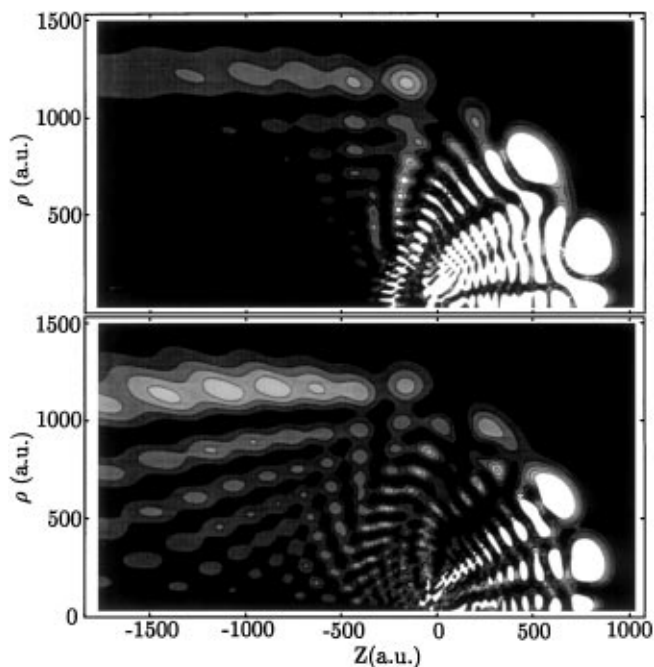


FIG. 3. Contour plot of the wave function (white at maxima) for the parameters of Figs. 1 and 2 with the upper figure at  $t = 3.5$  ps and the lower figure at  $t = 7.5$  ps.

The fold itself is apparent in the quantum calculation of the wave function as a ridge in Fig. 3 for  $1200 < \rho < 1300$  bohr. The region  $z < -500$  a.u.,  $\rho < 1500$  a.u. is classically allowed. It is somewhat spooky to note that the wave packet does not cover all of the classically allowed region downfield; it covers only those regions that a classical electron leaving the nucleus can reach.

We performed calculations for other experimental parameters and obtained good agreement with Ref. [11]. A fuller discussion of the different motions will be presented elsewhere. We note only one interesting case. An  $m = 1$  calculation for Rb had a substantial amount of probability return to the core in low  $\ell$  without substantial flux ejected. This situation arose because the amplitude for being ejected from  $\ell = 1$  interfered destructively with the amplitude for being ejected from  $\ell = 2$ . Just because the electron returns to the core with low  $\ell$  does not mean it will scatter downfield.

We thank G.M. Lankhuijzen and L.D. Noordam for providing us with their experimental data and for many profitable discussions. We gratefully acknowledge D. Harmin's help and insight. F.R. was supported by the NSF and J.S. was supported by the Department of Energy.

- 
- [1] A. ten Wolde, L.D. Noordam, A. Lagendijk, H.B. van Linden van den Heuvell, Phys. Rev. A **40**, 485 (1989).
  - [2] J.A. Yeazell and C.R. Stroud, Phys. Rev. Lett. **60**, 1494 (1988); J.A. Yeazell, M. Mallalieu, J. Parker, and C.R. Stroud, Phys. Rev. A **40**, 5040 (1989).
  - [3] A. ten Wolde, L.D. Noordam, H.G. Muller, A. Lagendijk, and H.B. van Linden van den Heuvell, Phys. Rev. Lett. **61**, 2099 (1988).
  - [4] J.A. Yeazell, M. Mallalieu, and C.R. Stroud, Phys. Rev. Lett. **64**, 2007 (1990); J.A. Yeazell and C.R. Stroud, Phys. Rev. A **43**, 5153 (1991).
  - [5] J.A. Yeazell and C.R. Stroud, Phys. Rev. A **35**, 2806 (1987); Phys. Rev. Lett. **60**, 1494 (1988).
  - [6] X. Wang and W.E. Cooke, Phys. Rev. Lett. **67**, 1496 (1991); Phys. Rev. A **46**, 4347 (1992).
  - [7] B. Broers, J.F. Christian, J.H. Hoogenraad, W.J. van der Zande, H.B. van Linden van den Heuvell, and L.D. Noordam, Phys. Rev. Lett. **71**, 344 (1993); B. Broers, J.F. Christian, and H.B. van Linden van den Heuvell, Phys. Rev. A **49**, 2498 (1994).
  - [8] H.H. Fielding, J. Wals, W.J. van der Zande, and H.B. van Linden van den Heuvell, Phys. Rev. A **51**, 611 (1995).
  - [9] R.R. Jones, C.S. Raman, D.W. Schumacher, and P.H. Bucksbaum, Phys. Rev. Lett. **71**, 2575 (1993).
  - [10] G.M. Lankhuijzen and L.D. Noordam, Phys. Rev. A **52**, 2016 (1995).
  - [11] G.M. Lankhuijzen and L.D. Noordam, Phys. Rev. Lett. **76**, 1784 (1996).
  - [12] D.A. Harmin, Phys. Rev. A **24**, 2491 (1981); **26**, 2656 (1982).
  - [13] U. Fano, Phys. Rev. A **24**, 619 (1981).
  - [14] J. Gao and J.B. Delos, Phys. Rev. A **49**, 869 (1994).
  - [15] M.L. Du and J.B. Delos, Phys. Rev. A **38**, 1913 (1988).